Journal of Magnetism and Magnetic Materials 559 (2022) 169543

Contents lists available at ScienceDirect

Journal of Magnetism and Magnetic Materials

journal homepage: www.elsevier.com/locate/jmmm

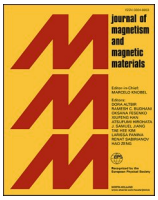

Effect of the distribution of anisotropy constants on the magnetic properties of iron oxide nanoparticles

D.M. Clarke [a], C. Marquina [b,c], D.C. Lloyd [d], G. Vallejo-Fernandez [a,*]

[a] Department of Physics, University of York, York YO10 5DD, UK
[b] Departamento de Física de la Materia Condensada, Universidad de Zaragoza, 50009-Zaragoza, Spain
[c] Instituto de Nanociencia y Materiales de Aragón (INMA); Consejo Superior de Investigaciones Científicas (CSIC)-Universidad de Zaragoza, 50009-Zaragoza, Spain
[d] Department of Electronic Engineering, University of York, York YO10 5DD, UK

ARTICLE INFO

Keywords:
Shape anisotropy
Magnetic hyperthermia
Iron oxide nanoparticles

ABSTRACT

The distribution of shape anisotropy constants in two colloids of iron oxide nanoparticles has been measured from the distribution of particle elongations within each system. The results are in good agreement with the values calculated from a temperature decay of remanence measurement. For a fluid with a saturation magnetisation of 420 emu/cc and an average particle elongation of ~ 1.3, the distribution of energy barriers is controlled by both the distribution of particle sizes and particle elongations. For a fluid with a saturation magnetisation of 320 emu/cc and a wide distribution of particle sizes, the energy barrier to reversal can be assumed to be controlled by the distribution of particle volumes. These results highlight the need to take into account the distribution of anisotropy constants when making predictions of the heating properties of assemblies of magnetic nanoparticles for hyperthermia applications.

1. Introduction

Over the last few decades, magnetic nanoparticles have gathered significant interest from the scientific community due to their promising application(s) in both medical diagnostics and therapeutics. Of particular interest are iron oxide nanoparticles due to their low toxicity, high biocompatibility and unique magnetic properties. For recent reviews on these topics see [1,2]. Magnetism is a volume science and, hence, the magnetic properties of such particles are controlled by their volume with many reports in the literature taking into account the distribution of particle sizes within a given system, e.g. [3]. However, the energy barrier to reversal is also controlled by the magnetic anisotropy constant of the material, K. In most reports, a constant value of K is assumed so that the distribution of energy barriers is taken to be solely controlled by the distribution of particle volumes. This is mainly due to the fact that measuring the distribution of anisotropy constants in a given system is significantly more complicated and time consuming than measuring the distribution of particle sizes. However, there are certain cases, e.g. magnetic nanoparticles with shape anisotropy, in which assuming a uniform value of K is an unrealistic assumption. In a recent work, we have shown that the distribution of anisotropy constants within an assembly of iron oxide nanoparticles can be determined successfully from electron microscopy from the measurement of the distribution of particle elongations within the system [4].

Magnetic hyperthermia is one of the applications of iron oxide nanoparticles that has attracted significant interest recently. When subjected to an alternating magnetic field, magnetic nanoparticles dissipate heat [5]. This heat can be used to cause cell necrosis within tumours. The technology is slowly starting to be adopted. For instance, MagForce AG have recently announced approval from the Food and Drug Administration (FDA) in the US to proceed with the final protocol of their pivotal US trial for the ablation of prostate cancer using their NanoTherm therapy system [6]. Their aim is to evaluate the use of their system in up to 100 patients for the treatment of prostate cancer with intermediate grade lesions. Hence, understanding and being able to predict the amount of heat generated by a given sample of magnetic nanoparticles at a given set of operating conditions is critical. However, it is also necessary to understand the limitations that might be present experimentally. For instance, it might not be possible to generate a field large enough to switch all the particles at the required frequency of operation over an extended area. There are many studies reporting on the different mechanisms controlling heat generation in magnetic nanoparticles but there seems to exist some consensus within the community that hysteresis losses are the dominant mechanism [7]. Hence, in

* Corresponding author.
E-mail address: gonzalo.vallejofernandez@york.ac.uk (G. Vallejo-Fernandez).

https://doi.org/10.1016/j.jmmm.2022.169543
Received 1 February 2022; Received in revised form 11 May 2022; Accepted 26 May 2022
Available online 28 May 2022

order to maximise heat generation, nanoparticles with a high saturation magnetisation and coercivity are required. This highlights the important role played by the magnetic anisotropy constant of the material. In this paper, we have investigated the effect of the distribution of anisotropy constants in two samples of iron oxide nanoparticles on their magnetic properties and the implications of such distribution for magnetic hyperthermia applications. The samples were chosen due to the different values of their saturation magnetisation (M_s) which, given the dependence of the shape anisotropy constant on M_s, will control the shape anisotropy constant of each material.

2. Methods

Iron oxide nanoparticles have a magnetocrystalline anisotropy of the order of $1.1x10^5$ erg/cc [8]. However, for cubic materials, the energy barrier to reversal is reduced by a factor of 4 (positive cubic anisotropy) or 12 (negative cubic anisotropy) compared to the uniaxial case [8]. Hence, their anisotropy is dominated by shape with the anisotropy constant for these materials being written as

$$K = \frac{1}{2}(N_a - N_c)M_s^2 \tag{1}$$

where N_a and N_c are the demagnetising factors [8]. In the case of a prolate spheroid N_a and N_c are given by

$$N_c = \frac{4\pi}{r^2-1}\left[\frac{r}{\sqrt{r^2-1}}\,ln\left(r+\sqrt{r^2-1}\right)-1\right]; N_a = \frac{4\pi - N_c}{2} \tag{2}$$

where r is the aspect ratio of the particle [8]. Using a value of M_s of 420 emu/cc, shape anisotropy becomes dominant for elongations greater than 5% [9]. The measurement of the anisotropy constant of any material and particularly magnetic nanoparticle systems is rather challenging. Gittleman [10] developed a technique that allows for the median value of the anisotropy constant to be determined from a measurement of the temperature decay of remanence. When the sample is cooled in zero field to a low enough temperature, the colloid will be frozen resulting in a randomly aligned system of blocked particles. Following the Stoner-Wohlfarth model for a system with uniaxial anisotropy, a remanence to saturation ratio $M_r/M_s = 0.5$ is expected at sufficiently low temperatures. The remanence at any temperature is then given by

$$\frac{M_r}{M_s} = 0.5\left(1 - \int_0^{V_P(T)} f(V)dV\right) \tag{3}$$

where $V_P(T)$ is the critical size for superparamagnetic behaviour at the temperature of measurement T. As the temperature is increased, the fraction of blocked particles in the distribution decreases resulting in a reduction of the remanence and, therefore, the remanence to saturation ratio. At the point at which the remanence has reached 50% of its low temperature value, half the volume of magnetic material in the colloid has become superparamagnetic. Assuming the particle size distribution is known to high accuracy, the median value of the anisotropy constant, K_m, can be calculated following

$$K_m = \frac{\ln(t_m f_0)k_B T_b}{V_m} \tag{4}$$

where t_m is the waiting time at zero field before the remanence is measured, f_0 is the attempt frequency taken as $10^9\ s^{-1}$, k_B is Boltzmanns' constant, T_b is the temperature of measurement and V_m is the median volume within the sample. Similarly, the variation of the coercivity with the maximum applied field is given by [11]

$$\frac{H_c(T)}{H_c^{max}} = \left[1 - \sqrt{\frac{\ln(tf_0)k_B T}{KV_m^{'}(T)}}\right] \bullet \int_{V_P(T)}^{V_{crit}(T)} f(V)dV \tag{5}$$

where t in this case is the time of measurement, H_c^{max} the coercivity of the system when the maximum applied field is large enough to saturate the entire sample and V_{crit} represents the maximum volume that can be switched for a given applied field. $V_m^{'}$ is the volume that satisfies.

$$\frac{\int_{V_P(T)}^{V_m^{'}(T)} f(V)dV}{\int_{V_P(T)}^{V_{crit}(T)} f(V)dV} = 0.5 \tag{6}$$

At sufficiently low temperatures and when the magnetisation of all the particles can be switched, $V_m^{'}$ coincides with the median particle volume.

The above mathematical approach is only valid when the distribution of anisotropy constants, g(K), is very narrow. More generally, the temperature at which the remanence reaches half of its maximum value equates to the median value of the energy barrier to reversal ΔE_m. Hence, Eq. (3) has to be rewritten as

$$\frac{M_r}{M_s} = 0.5\left(1 - \int_0^{\infty}\int_0^{\infty} f(V)g(K)\delta(K,V)dVdK\right) \tag{7}$$

where δ(K,V) is a delta type function that is equal to 1 if a given particle is blocked at a specific temperature and 0 otherwise. Similarly, Eq. (5) needs to be rewritten in terms of the energy barrier to reversal rather than just the volume.

$$\frac{H_c(T)}{H_c^{max}} = \left[1 - \sqrt{\frac{\ln(tf_0)k_B T}{\Delta E_m^{'}(T)}}\right] \bullet \int_{\Delta E_P(T)}^{\Delta E_{crit}(T)} f(\Delta E)d(\Delta E) \tag{8}$$

where $\Delta E_m^{'}(T)$, $\Delta E_p(T)$ and $\Delta E_{crit}(T)$ are equivalent terms to $V_m^{'}$, $V_p(T)$ and $V_{crit}(T)$ in Eq. (5).

3. Experimental results

Two different samples of iron oxide nanoparticles have been studied in this work. The materials were prepared by Liquids Research Ltd. following a variation of the well known co-precipitation method [12]. The main difference between both samples was the saturation magnetisation of the resulting fluid and their respective particle size distributions. An initial sample (general fluid) was first prepared resulting in a saturation magnetisation of 320 emu/cc. These particles were then subjected to what is known as the Controlled Growth Process (CGP) which results in nanoparticles with a saturation magnetisation of 420 emu/cc and a narrow particle size distribution. These high moment nanoparticles receive the brand name HyperMAG®C [13]. Fig. 1(a) and (g) show a typical TEM image and particle size distribution for the general, low M_s, fluid while Fig. 1(b) and (h) show the equivalent data for the HyperMAG® fluid. Fig. 1(c) and (d) show a high resolution TEM image for each sample while Fig. 1 (e) and (f) show a selected area diffraction pattern for each sample. From these data, it is clear that the same crystalline phases are present in both samples. The presence of bright spots in the diffraction pattern for the HyperMAG® sample is an indication of the larger crystallites present in this sample which is consistent with the particle size distribution data shown at the bottom of Fig. 1.

The particle size distribution for each sample was measured from transmission electron microscope (TEM) images such as those shown in Fig. 1 (a) and (b). The images were taken using a JEOL 2100 + TEM with an accelerating voltage of 200 keV. Multiple images from different regions in the grid were obtained and 500 particles were measured for each sample. Two different methods were used to measure the particle size distribution in each sample. A Zeiss particle size analyser was used which consists of a light box with a variable aperture. The resulting circular beam of light was used to obtain the particle diameter via an equivalent circle method. The distribution was also measured using ImageJ software [14]. This allowed for not only the particle size to be recorded but also the particle elongation to be measured allowing for the

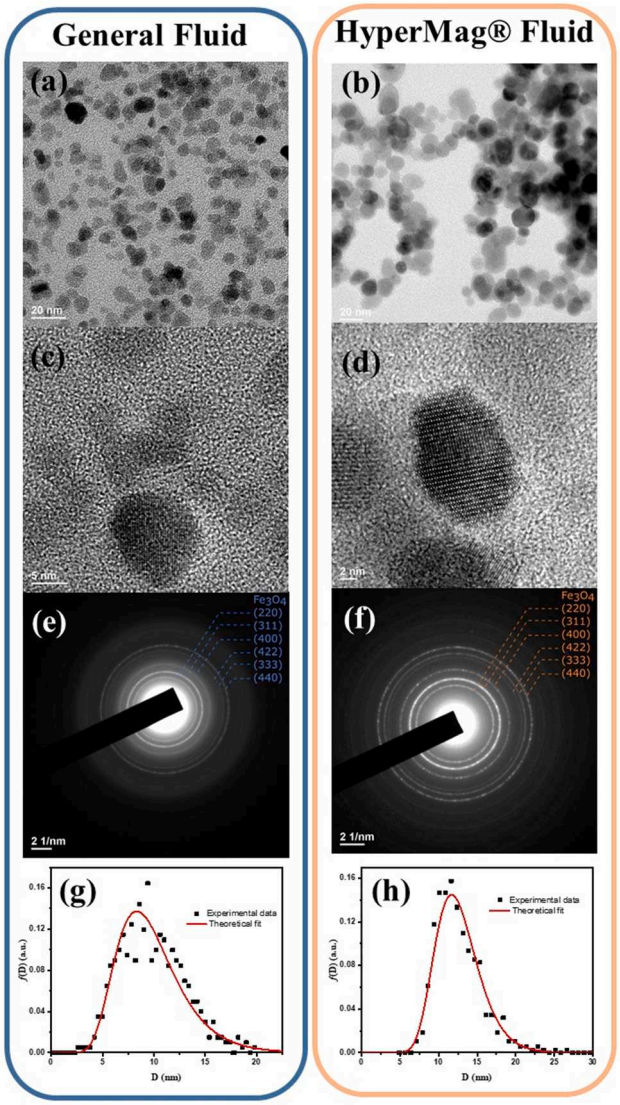

Fig. 1. (a) and (b) Bright field TEM images; (c) and (d) High resolution TEM images; (e) and (f) Selected area diffraction patterns; (g) and (h) Particle size distributions for both samples.

correlation between particle size and particle elongation to be determined. The results from both measurement techniques for each sample were in excellent agreement with differences in the median particle size and the standard deviation of the distribution agreeing within error. In both cases the diameters followed a lognormal distribution with a median diameter D_m = 9.3/12.3 nm and a standard deviation σ = 0.33/0.23 for the general/HyperMAG® fluid, respectively. As expected the median particle size for the general fluid was smaller than that for the HyperMAG® sample. For our calculations the presence of a magnetic dead layer, 2 atoms thick, on the surface of the particles was taken into account [4].

As mentioned above, the particle elongation was measured using ImageJ by determining the ratio of the maximum number of pixels in a given particle to the minimum number, in a direction approximately orthogonal to the long axis of the particle. Fig. 2 shows the particle elongation as a function of particle size for both systems. The error bars in the figure correspond to the standard deviation after binning the data. There is an increase in the particle elongation with increasing particle size for both samples. For our calculations, we have applied a linear correction so that larger particles were assumed to have a larger average elongation using the data in Fig. 2. The standard deviation of the

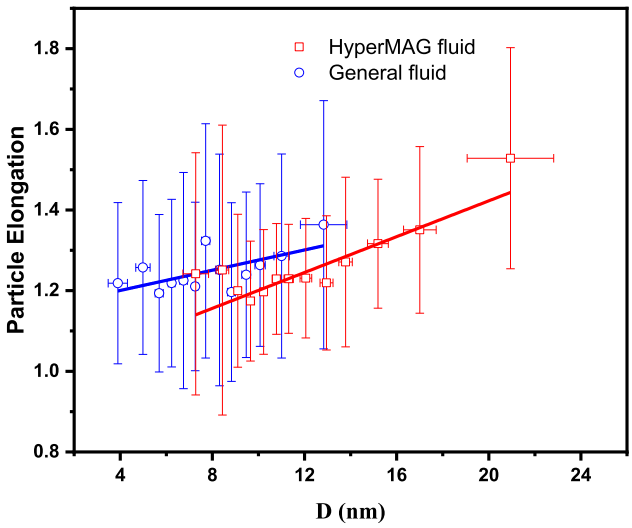

Fig. 2. Particle elongation as a function of particle size for both fluids studied in this work.

elongation does not seem to depend on the particle size while the standard deviation in the particle size is significantly larger for the bigger particles in the distribution. This is due to the fewer particles that could be measured in that range compared for instance with the availability of particles with a size in the centre of the distribution. From the data in Fig. 2 and Eq. (1) a median value of the anisotropy constant was determined for each particle size. In each case the distribution of anisotropy constants was assumed to be Gaussian with the standard deviation for each distribution calculated from the data in Fig. 2 and assumed to be the same for all particle sizes. Using the elongation data shown in Fig. 2 a median value of the anisotropy constant of 0.4×10^5 and 1.3×10^5 erg/cc was calculated for the general and HyperMAG® fluids, respectively.

The CGP not only results in an increase in the median particle size but also in a dramatic decrease in the width of the distribution. The standard deviation of the lognormal fit decreases from 0.33 for the general fluid to 0.23 for the HyperMAG® sample. Hence, it could be argued that, given the lower value of M_s and the measured distribution of particle elongations for the general fluid, the distribution of energy barriers in this system will be controlled to a first approximation by the distribution of particle volumes while for the HyperMAG® fluid, both the distribution of particle sizes and elongations will need to be considered. In order to verify this assumption, the temperature decay of remanence as well as the high frequency magnetic response for both samples have been measured.

The samples were initially cooled in zero field to 1.8 K using a SQUID magnetometer fitted with a continuous flow cryostat. A hysteresis loop, shown in Fig. 3, including the initial magnetising curve for each sample was measured at that temperature after saturation in a maximum applied field of 50 kOe. The coercivity of the samples were 267 Oe and 303 Oe for the general and HyperMAG® fluids, respectively. At that temperature, the coercivity of the samples should be $\sim 0.96 K_m/M_s$, i.e. the anisotropy field for a system of randomly oriented particles with uniaxial anisotropy [15]. Given that the anisotropy of these systems is controlled by shape and, assuming that the elongation of the particles in both samples is similar, the coercivity should be proportional to the saturation magnetisation of the material. The higher coercivity measured for the HyperMAG® fluid is consistent with this interpretation. From the closing point of both hysteresis loops (~2 kOe) a field of 5 kOe was deemed adequate to switch all the blocked particles even at this low temperature. Hence, for the temperature decay of remanence the samples were saturated in a field of 5 kOe. The field was then removed and the remanence measured after waiting for 100 s. The temperature

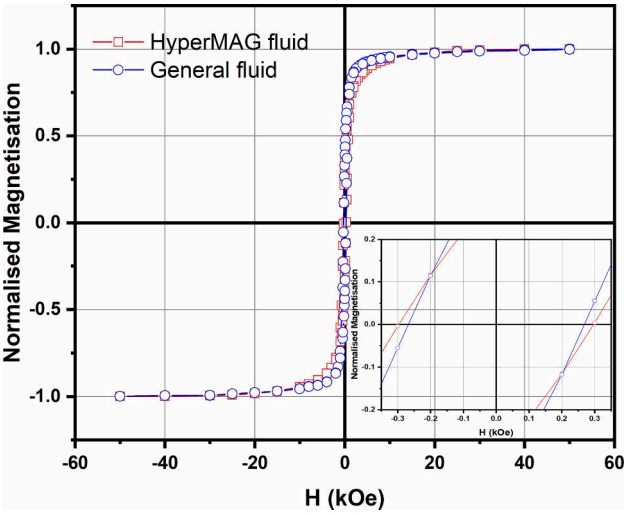

Fig. 3. Hysteresis loop measured for each sample at 1.8 K.

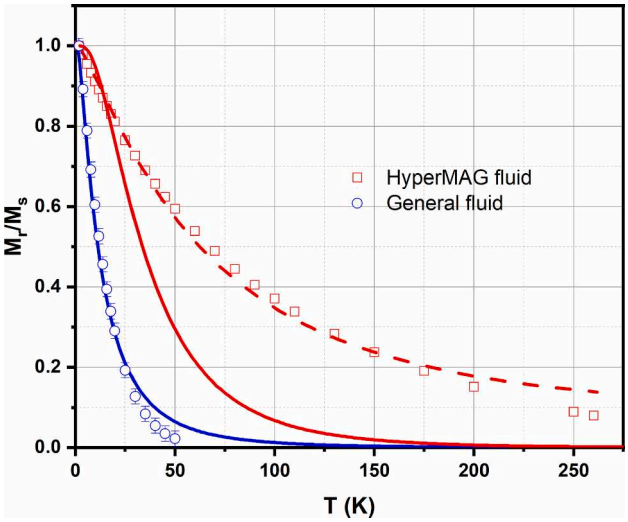

Fig. 4. Temperature decay of remanence for the samples studied in this work. The solid line for the general/HyperMAG® fluid assumes a uniform value of K while the dashed red line corresponds to the fit for the HyperMAG® fluid assuming a non-uniform value of K.

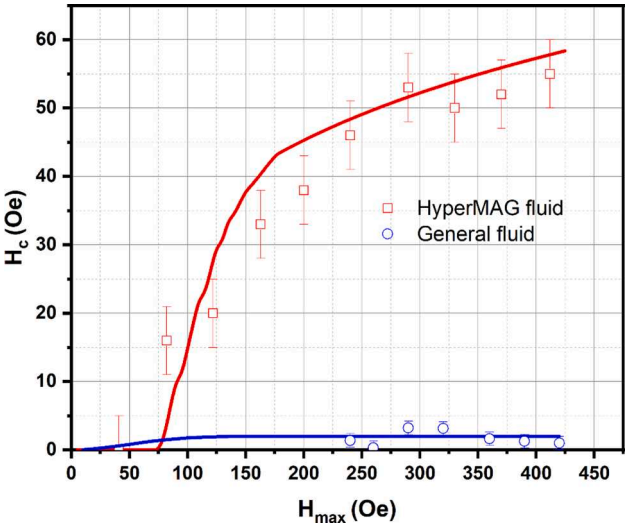

Fig. 5. Coercivity as a function of maximum applied field for both samples measured at 47 kHz. The solid lines were calculated using Eq. (5) for the general fluid and Eq. (8) for the HyperMAG® fluid.

was then raised in 2–5 K steps and the remanence measured after re-saturating the sample. This is the same measurement procedure we have used in the past [4]. The 50% point in the temperature decay of remanence in Fig. 4 occurs at a temperature $T_b = (62 \pm 2)$ K for the HyperMAG® fluid and (11 ± 2) K for the general fluid. These values result in a median value of the anisotropy constant of 1.29×10^5 erg/cc and 0.36×10^5 erg/cc for the HyperMAG® and general fluids, respectively. For our calculations we have deemed that the point at which half the magnetic volume had become superparamagnetic was that at which the value of the remanence was equal to half that at 1.8 K. Fig. 4 shows the temperature decay of remanence for both samples. The solid lines in Fig. 4 correspond to the theoretical fits using Eq. (3), which assumes a uniform value of K, for both samples. In the case of the HyperMAG® fluid, a value of $K = 1.29 \times 10^5$erg/cc was assumed. The fit for this sample is very poor. The dashed line in Fig. 4 shows the calculated fit for the HyperMAG® sample using Eq. (7) which takes into account the distribution of anisotropy constants in the sample. The distribution was assumed to be Gaussian [4] with the parameters for the distribution taken from the data in Fig. 2. The parameters required in Eqns. (3) and (7) were determined experimentally from the data shown in Figs. 1 and 2 and the measurement conditions in the magnetometer, i.e. $t_m = 100$ s. It is clear from this data that the distribution of anisotropy constants cannot be ignored for the HyperMAG® fluid.

The coervivity of the particles as a function of the applied field has been measured at 47 kHz using a high frequency loop tracer developed in our group [16]. The system is based on a resonant circuit with the inclusion of three MnZn ferrite rods inside the primary coil which enhances the field available by up to a factor 6 compared to the case when no ferrites are present. By tuning the current through the primary coil in the range 0–2.5 A fields in the range 0–420 Oe can be achieved at a range of operating frequencies. Fig. 5 shows the coercivity of both samples as a function of the maximum applied field. The solid lines were calculated using Eq. (8). The same fitting parameters used for previous calculations were used to obtain the fits in Fig. 5. Very good agreement is obtained again in both cases. Based on these data and the saturation magnetisation values for each sample, it is clear that the HyperMAG® fluid would be significantly more effective at generating heat than the general fluid. In addition, in order to predict the hystereric losses in the HyperMAG® fluid, knowledge of the distribution of anisotropy constants is essential.

4. Conclusions

In conclusion, we have shown that the distribution of anisotropy constants ought to be taken into account when studying the magnetic response of assemblies of iron oxide nanoparticles or any other magnetic system where shape anisotropy dominates. This is particularly important when studying the suitability of such nanoparticles for magnetic hyperthermia applications where hysteresis losses control the amount of heat being generated. The energy barrier to reversal in such systems cannot be assumed to be controlled solely by the distribution of particle volumes. If the distribution of anisotropy constants were not to be taken into account, it would not be possible to make meaningful predictions of the amount of heat being generated at a given field amplitude and frequency of operation.

Declaration of Competing Interest

The authors declare that they have no known competing financial interests or personal relationships that could have appeared to influence the work reported in this paper.

Acknowledgements

The authors acknowledge fruitful discussions with Prof. Kevin O'Grady (emeritus) from the Department of Physics at the University of York and Liquids Research Ltd. Generous financial support from Liquids Research Ltd. is also greatly appreciated. The authors acknowledge TEM support from Prof. A. Hirohata from the Electronic Engineering department at the University of York. Funding is also acknowledged from EPSRC via their Impact Acceleration Account (EP/R51181X/1). The authors would like to acknowledge the use of Servicio General de Apoyo a la Investigación-SAI at Universidad de Zaragoza. These results/ publication are part of the project PID2019-106947RB- C21 financed by MCIN/ AEI /10.13039/501100011033. CM also acknowledges financial support from the Regional Government of Aragón (DGA) for financial support through grant E28_20R.

References

[1] A. Ali, T. Shah, R. Ullah, P. Zhou, M. Guo, M. Ovais, Z. Tan, Y. Rui, Front. Chem. 9 (2021), 629054.
[2] I. Rubia-Rodriguez, A. Santana-Otero, S. Spassov, E. Tombácz, C. Johansson, P. De La Presa, F. J. Teran, M. del Puerto Morales, S. Veintemillas-Verdaguer, N. T. K. Thanh, M. O. Besenahard, C. Wilhelm, F. Gazeau, Q. Harmer, E, Mayes, B. B. Manshian, S. J. Soenen, Y. Gu, A. Millan, E. K. Efthimiadou, J. Gaudet, P. Goodwill, J. Mansfield, U. Steinhoff, J. Wells, F. Wiekhorst, and D. Ortega, Materials 14, 706 (2021).
[3] M. El-Hilo, K. O'Grady, R.W. Chantrell, J. Magn. Magn. Mater. 114 (1992) 295.
[4] A.A. McGhie, C. Marquina, K. O'Grady, G. Vallejo-Fernandez, J. Phys. D: Appl. Phys. 50 (2017), 455003.
[5] E. Lima Jr., T.E. Torres, L.M. Rossi, H.R. Rechenberg, T.S. Berquo, A. Ibarra, C. Marquina, M.R. Ibarra, G.F. Goya, J. Nanopart. Res. 15 (2013) 1654.
[6] https://www.magforce.com/en/news/?article=361 (accessed on December 13 2021).
[7] K. Mahmoudi, A. Bouras, D. Bozec, R. Ivbkov, C. Hadjipanayis, Int. J. Hyperthermia 34 (2018) 1316.
[8] B.D. Cullity, C.D. Graham (Eds.), Introduction to Magnetic Materials, John Wiley & Sons, Inc., Hoboken, NJ, USA, 2008.
[9] G. Vallejo-Fernandez, K. O'Grady, Appl. Phys. Lett. 103 (2013), 142417.
[10] J.I. Gittleman, B. Abeles, S. Bozowski, Phys. Rev. 9 (1974) 3891.
[11] G. Vallejo-Fernandez, A.G. Roca, K. O'Grady, IEEE Trans. Magn. 47 (2011) 2878.
[12] S.E. Khalafalla, G.W. Reimens, IEEE Trans. Magn. 16 (1980) 178.
[13] https://www.liquidsresearch.com.
[14] https://imagej.nih.gov/ij/.
[15] F.E. Luborsky, J. Appl. Phys. 32 (1961) 171S.
[16] D.M. Clarke, G. Vallejo Fernandez, J. Magn. Magn. Mater. 552 (2022), 169249.